



UNIVERSITÀ POLITECNICA DELLE MARCHE
Repository ISTITUZIONALE

Automatic monitoring of the bio-colonisation of historical building's facades through convolutional neural networks (CNN)

This is a pre print version of the following article:

Original

Automatic monitoring of the bio-colonisation of historical building's facades through convolutional neural networks (CNN) / D'Orazio, Marco; Gianangeli, Andrea; Monni, Francesco; Quagliarini, Enrico. - In: JOURNAL OF CULTURAL HERITAGE. - ISSN 1296-2074. - 70:(2024), pp. 80-89. [10.1016/j.culher.2024.08.012]

Availability:

This version is available at: 11566/336113 since: 2024-10-16T11:13:18Z

Publisher:

Published

DOI:10.1016/j.culher.2024.08.012

Terms of use:

The terms and conditions for the reuse of this version of the manuscript are specified in the publishing policy. The use of copyrighted works requires the consent of the rights' holder (author or publisher). Works made available under a Creative Commons license or a Publisher's custom-made license can be used according to the terms and conditions contained therein. See editor's website for further information and terms and conditions.

This item was downloaded from IRIS Università Politecnica delle Marche (<https://iris.univpm.it>). When citing, please refer to the published version.

(Article begins on next page)

AUTOMATIC MONITORING OF THE BIODETERIORATION OF HISTORICAL BUILDING'S FACADES THROUGH CONVOLUTIONAL NEURAL NETWORKS (CNN)

Marco D'Orazio^{a*}, Andrea Gianangeli^a, Francesco Monni^a, Enrico Quagliarini^a

^a Department of Construction, Civil Engineering and Architecture (DICEA), Università Politecnica delle Marche, via
Brecce Bianche, 60131 Ancona, Italy

* Corresponding author, Tel: +39 0712204587.

Email addresses: m.dorazio@univpm.it (M. D'Orazio), a.gianangeli@univpm.it (A. Gianangeli), f.monni@univpm.it
(F. Monni), e.quagliarini@univpm.it (E. Quagliarini)

ABSTRACT

Built cultural heritage is exposed to various deterioration problems caused by different types of actions. To reduce the need for major interventions, preventive conservation (PC) approaches were proposed, based on data collection, regular monitoring, inspections, and control of environmental factors. Monitoring actions able to depict the evolution of buildings' deterioration state, have been proposed and implemented in real cases. Considering that digital images (DI) of historical facades are constantly collected by different subjects and for different purposes, they represent the widest existing data source to support PC approaches and develop predictive tools. DI of historical façades can be used to help in the early recognition of different types of deterioration processes, supporting the creation and application of predictive models based on machine learning (ML) methods. This work proposes a method for the early detection of biological colonization of building facades. A convolutional neural network (CNN) has been trained and tested with images representing the microalgae growth process on historical bricks' facades, collected during experimental activities in controlled conditions. The trained model is characterized by an accuracy of 83% and can recognize the starts of the bio-colonization process on different types of bricks. The trained model has been applied to a historical building used as a case study. The facades of the case study are constantly monitored by surveillance cameras, and DI of the facades are often collected due to the public function of the building. The study shows that by simply processing these images with the trained network it is possible to detect the first stage of bio-deterioration processes. This work is part of a more extensive research for the early detection of different types of building façade damages and can be easily implemented where DI coming from surveillance cameras or other sources are available.

Keywords

Microalgae, biodeterioration, historical buildings, convolutional neural network, monitoring

1 INTRODUCTION

1 Since the end of the last century, cultural heritage has been increasingly recognized as an important and
2 strategic resource for a sustainable development, and the awareness of its potential for the socio-economic
3 progress of society has constantly grown [1]. Building heritage, due to its material nature, is markedly affected
4 by the factors that contribute to its degradation: physical, chemical, natural and human actions [2].

5 To preserve this heritage that has come down to us from the past, it is necessary to have intervention
6 strategies tailored for specificities of this field. To this end, it is widely accepted that the PC can be considered
7 the most cost-effective strategy, strongly recommended by international institutions involved in preservation
8 [3]. PC means implementing a strategy of care, based on data collection, regular monitoring, inspections,
9 control of environmental factors and maintenance activities [4]. This concept can be resumed as “a set of
10 actions useful for reducing risk situations concerning cultural assets in their context” [5] [6]. The PC approach
11 starts from a “medical analogy” between the diagnostic process for human and building pathologies [7]. So,
12 following this analogy, damages and defects can be seen as symptoms of a pathology, and therefore a key
13 part of a PC approach is the development of effective “early” damage detection systems, based on the
14 continuous surveillance (i.e., data collection, monitoring activities) of the architectural heritage.

15 Among the various pathologies that can afflict architectural heritage, attention must certainly be paid to the
16 growth of living microorganisms (bio-colonization). Almost all the historical buildings are affected by primary,
17 secondary or tertiary colonizers such as microalgae (primary), molds, lichens (secondary), plants (tertiary),
18 causing permanent alterations of building facades and relevant costs. The interaction between environmental
19 factors and the physical and chemical properties of masonry could be the starting point for a colonization
20 process by primary colonizers, such as microalgae [8][9][10]. The development of these microorganisms has
21 a direct consequence on the material characteristics which are inevitably increasingly degraded with the
22 passage of time and therefore with growth of living organisms that could cause serious losses (especially in
23 the case of cultural heritage buildings) [11]–[16]. Fungi, mould, cyanobacteria, and green microalgae [17] can
24 grow depending on several factors, especially temperature and availability of water, producing chemical and
25 physical degradation of the façade material and becoming a suitable substrate for the growth of other
26 colonizers [18], such as mosses and lichens [8][19][20]. Biological fouling usually starts with the colonization
27 by photoautotrophic microorganisms [8][20] Green microalgae and cyanobacteria (microalgae) are recurrent
28 and they usually develop in combination [9], [21]–[23]. Microalgae can survive at atmospheric temperatures
29 of 5-35/40°C, in rainy, winter and spring seasons. Microalgae require water, but can survive for years to
30 extreme desiccation states and recover full metabolic activity within few hours after rewetting [24].
31 Roughness and porosity can promote algae growth [25]–[27].

32 To limit aesthetical, chemical and physical degradation due to bio-colonizers, early detection systems based
33 on data and image collection can be useful.

34 In the last years many researchers have focused their attention on computer vision-based automated building

pathologies identification (using image processing and ML techniques).

An issue that has received a lot of attention is the one of crack detection. Munawar et al. [28] presented a review of image-based crack detection techniques which implement image processing and/or ML. Many works focus on concrete crack detection [29]–[33], not only in the field of existing building but also in the one of infrastructures, like bridges [34]–[39] or roads [40]–[43]. Rezaie et al. [44], Minh Dang et al. [45], Loverdos and Sarhosis [46] focus their works on masonry crack detection.

Several studies oriented on architectural heritage for the automated identification of masonry surface damages by photographing the structure and using ML techniques have also been conducted. Wang et al. [47], [48] used CNN classification techniques to identify and locate several types of damages (like cracks, efflorescence, and spalling) in brick-masonry walls. Remaining in the field of cultural heritage, Wang et al. [49] used CNN for damage identification - such as spalling and area loss - in the roof tiles of a historical building. Zou et al. [50] used CNN to automate the detection of missing components in heritage buildings with particular attention to preventive maintenance activities.

As regard the problem of historical buildings affected by tertiary colonizers (plants) has been addressed the work developed by Ottoni et al. [51] in which is proposed a method for automatic recognition of vegetation on building facades and roofs. Hatir et al. [52] proposed a deep learning method for detection and mapping of stone deterioration in archaeological heritage sites, including the presence of biological colonization.

Regarding the specific identification of microalgae, Chong et al. [53] presents a state-of-the-art of identification methods and ML techniques for image analysis. Pre-processing actions (i.e., resizing, grey-scaling, denoising) and feature extraction methods to apply ML methods (i.e., ANN, CNN, K-NN, DL, SVM) were analysed in depth. The Chong's work shows that CNN (convolutional neural networks) are widely used to identify different types of microalgae species based on DI. However, cited works [54]–[63] are mainly based on images acquired during the growth of microalgae strains in water solution and not on building facades.

The recognition of microalgae on building facades has been analysed in previous works but not in the case of historical facing-masonry walls. In fact, Tran and Hoang [64], [65] proposed a method based on ML techniques for predicting the appearance of algae on building's facades, but in presence of mortar cladding. Valença et al. [66], [67] presented a method designed to detect, analyse and measure areas with biological colonization in exposed concrete surfaces. Considering lack of existing literature, this paper proposes the creation and application of predictive models using CNN able to automatically monitor the biodeterioration status of historical building facades, acting as early detection system.

2 RESEARCH AIM

Following similar approaches where the availability of DI obtained for other purposes is used to detect specific damages [68], and considering that DI of historical facades are constantly collected for different purposes (i.e. surveillance), the aim of present work is to check the ability of a CNN to recognize the growth of microalgae

1 on real images of building facades. Firstly, the CNN was trained using images obtained from an experimental
2 activity and then was applied to a case study to check if the model can recognize microalgae on historical
3 surfaces using common DI (from surveillance cameras or manually collected). The results show as the model
4 trained with laboratory images is able to detect the starts of bio-colonization process with good accuracy. If
5 applied to the case study the method shows a loss of accuracy. It has to be said that the use of common DI
6 could be considered a challenge in several aspects: presence of other elements (e.g., ground, roofs, etc.), low
7 quality, misalignment respect to wall surface plane, significant variation of illuminance. The results can be
8 considered as a starting point towards the creation of tools for early detection of building facades damages
9 using common imagines easy to find.
10
11
12
13
14
15
16

17 **3 MATERIALS AND METHODS**

18 **3.1 Research framework**

19 A four-step research framework has been developed to reach the proposed aim: early identification of bio-
20 deterioration processes on historical building facades. Firstly, an experimental activity (see 3.2) has been
21 organized to follow, in controlled conditions, the microalgae growth process, considering different types of
22 bricks used in the past to realize historical buildings and different types of exposures (temperature, RH%,
23 rain). Then, DI collected during the experimental activity were resized and cropped to obtain a dataset of
24 about 12.000 sub-images (see 3.3), representing the different stages of the bio-deterioration process, and a
25 CNN was trained and tested with the DI dataset obtaining high accuracy (see 3.4). Finally (phase 4), video and
26 DI periodically collected by surveillance cameras during the normal life of an historic building were used to
27 check the ability of the trained network to work in a real case (see 3.5). The whole research framework is
28 depicted in Figure 1.
29
30
31
32
33
34
35
36
37
38
39
40

41 **3.2 Experimental activity**

42 An extended experimental campaign was arranged to obtain the images useful to train the CNN. Five different
43 types of clay bricks (named AH, AL, B, CH and CL) were selected and tested in five different environmental
44 conditions, reproduced using climatic chambers to accelerate the growth process. Bricks differ by color and
45 microstructure (porosity, roughness). Three different brick's colors (light-red, dark-red, yellow) were chosen
46 considering that bio-colonization causes a shift of the original color towards green-blue nuances, and the
47 initial color spectrum is influenced by the shift in wetted and unwetted conditions. Different microstructures
48 were considered because the "shape" of the bio-colonization (i.e., spots, lines, areas) is influenced by the
49 surface characteristics and the water retention ability of the bricks. Finally, different environmental conditions
50 characterized by different temperatures, RH%, and wetting processes were considered to include a wide
51 range of the expected environmental conditions.
52
53
54
55
56
57
58
59
60
61
62
63
64
65

1 To characterize surface properties of the bricks, porosity and roughness were preliminary measured. The total
2 open porosity P [%] was determined by a mercury intrusion porosimeter (Micromeritics Autopore III)
3 according to the ASTM D4404-10 standard [69]. The surface roughness R_a [μm] was measured according to
4 UNI EN ISO 4287:2009 standard [70], by using a Taylor Hobson CCI 3D Optical Profiler (Table 1).
5

6 To reproduce the bio-colonization process, a green alga (*Chlorella mirabilis* strain ALCP 221B) and a
7 cyanobacterium (*Chroococcidiopsis fissurarum* strain IPPAS B445) were chosen [20], [71], [72]. Microbial
8 strains were cultivated in a Bold's Basal Medium (BBM) prepared in accordance with ASTM D5589-09
9 standard method [73]. Since a visible biological degradation mostly starts [18] after 1-year or more of natural
10 environmental exposure [74], [75], the use of accelerated tests is recommended. Five different environmental
11 conditions were chosen to consider a wide range of possible real exposures. Three different relative humidity
12 (RH) conditions were reproduced in three separate climatic chambers to investigate their effect on algae
13 growth on fired brick surfaces. The indoor environment was conditioned by saturated solutions, as indicated
14 in EN ISO 12571:2013 [76]. The RH_1 (about 75%) was obtained through a saturated solution of NaCl, RH_2
15 (about 87%) through a saturated solution of Na_2CO_3 , and RH_3 (about 98%) through only deionized water [77].
16 To only consider the effect of RH, temperature was maintained at 27.5 ± 2.5 °C during all the tests. At the
17 beginning of the test, 9 different points on the surface of each sample were inoculated with 5 μL of the mixed
18 culture per point. After the initial inoculation, samples were positioned inside the climatic chambers, inclined
19 at 45° on aluminum-glass racks, front-to-front along the long dimension of the chamber. The test apparatus
20 was placed in a closed room to avoid the influence of light, temperature, and RH of the external environment.
21 Each growth chamber was equipped with two neon lamps (Sylvania TopLife 39W) to provide an adequate
22 illumination equivalent to day/night cycles 14/10 h (Figure 2a).
23

24 The influence of temperature on algae growth was carried out following previous researches [25], [26], [72],
25 [78]. Accelerated tests with a periodical water spray on the material surface were performed until the
26 stagnation phase was reached (Figure 2b). Test apparatus consisted of growth chambers ($100 \times 40 \times 53$ cm³),
27 filled with 35L of BBM inoculated with the mixed cultures. Algal suspension was sprinkled on sample surfaces
28 (8×8 cm²) positioned above two aluminum-glass composed racks inclined at 45°. Run/off cycles were set at
29 intervals lasting 15 min and a total of 6 hours per day (3 hours run and 3 hours off). A day/night illumination
30 cycles (14/10 h) were provided by two 39 W neon lamps (Sylvania TopLife).
31

32 Considering the available literature [79]–[85], the accelerated tests were set under two different
33 temperatures: 27.5 ± 2.5 °C, that is a temperature within the range of the optimal growth values comprised
34 between 20 °C and 30 °C [79]–[83], and a lower value equal to 10 ± 2.5 °C, within the range of suitable growth
35 [84], [85]. To set the lower test temperature, a modified refrigerator (Electrolux RC 5200 AOW2) was used.
36 Relative humidity was assumed constantly equal to 100% due to the wetting cycles. All the test environments
37 were monitored by temperature and RH sensors (Sensirion SHT31-D), through measurements every 10
38 minutes.
39
40
41
42
43
44
45
46
47
48
49
50
51
52
53
54
55
56
57
58
59
60
61
62
63
64
65

1
2
3 During each accelerated growth test, analyses were carried out for the evaluation of the algal extent and the
4 biofouling process on samples' surface [25]. Firstly, colorimetric analysis was performed to examine the color
5 variation during time. The chromatic variation (ΔE) was measured with a spectrophotometer (Konika Minolta
6 CM-2600dD) [72], [86]. In accordance with UNI EN 15886:2010 and UNI 1602371:2018, results were
7 expressed in CIELAB color space [87], [88]. Color variation was calculated in terms of total color difference ΔE ,
8 by equation (1):
9

$$\Delta E = \sqrt{(L_0^* - L^*)^2 + (a_0^* - a^*)^2 + (b_0^* - b^*)^2} \quad (1)$$

10
11 where L_0^* , a_0^* , b_0^* are the color coordinates of samples before the beginning of the test (time zero), and L^* ,
12 a^* , b^* the ones measured during the accelerated growth. Measurements were repeated on nine points on
13 each sample surface about every week.
14
15
16
17
18
19
20
21
22
23

24 **3.3 Image acquisition and splitting**

25
26 Finally, to train the CNN, DI were weekly collected through a high-resolution scanner (HP Scanjet G3010). The
27 effectiveness of this method has been confirmed in previous studies [9], [25]. The acquired images were
28 elaborated with Imagemagick software as described in the following section. All the images were resized to
29 1780x1780 pixels using the "imagemagick" tool, rel.7.1.1-20, then cropped to obtain 256x256 sub-images.
30 From each image, 49 sub-images were obtained. All the sub-images were randomly renamed and reordered.
31 Then a manual annotation process was performed. To facilitate the annotation process and considering that
32 microalgae growth causes a color shift towards green values, the image's R, G and B channels were filtered
33 using Matlab software (rel. 2023a). Images showing traces of microalgae were annotated as "algae", and the
34 others as "no_algae". Finally, the annotated dataset of images, consisting of 13.120 sub-images was equally
35 divided into 2 parts, "train" and "test". Each part of the dataset comprises 4780 "algae" images and 1780
36 "no_algae" images. No filtering actions were performed on resulting images, to check the capability of the
37 trained and tested CNN to work directly with real images [63].
38
39
40
41
42
43
44
45
46
47
48

49 **3.4 Convolutional network design, training and testing**

50
51 A CNN, is a deep learning neural network designed for processing structured arrays of data. CNNs has been
52 successfully applied to various computer vision applications, especially for analyzing visual images and for the
53 multi-category classification (categorizing samples into one of three or more classes) [64]–[68]. A CNN is a
54 feed-forward neural network, comprising many convolutional layers stacked on top of each other, each one
55 capable of recognizing more sophisticated shapes. Pooling layers (subsampling layers) are included. The
56 pooling layer replaces the output of the network at certain locations by deriving a summary statistic of the
57
58
59
60
61
62
63
64
65

1 nearby outputs. This helps in reducing the spatial size of the representation, which decreases the required
2 amount of computation and weights. After a hyper-tuning process, addressed to optimize the number of
3 layers of the CNN a Two-convolution layers CNN was chosen. The first convolutional layer has dimension [32,
4 (3,3)]. The second convolutional layer has the dimension [64, (3,3)] Two pooling layers were included and
5 finally a flatten layer, necessary to convert the resulting matrix into a single array and two dense layers (256,1)
6 have been included. “Relu” activation function has been chosen for the convolutional layers and for the first
7 dense layer. “Sigmoid” activation function has been chosen for the second “dense” layer. RMSprop optimizer
8 (learning rate = 0.001) has been considered. Considering that we have a binary classification problem,
9 accuracy metric was plotted. Accuracy is the ratio of the number of correct predictions to the total number
10 of predictions made by the model. A batch size of 20 and 50 epochs, for the training process were considered.
11 To train and test the CNN a python script (rel 3.9) has been written. “Tensorflow” and “Keras” libraries were
12 used to train and test the CNN, “Keras-tuner” library has been used to hyper-tune (parameter optimization)
13 the neural network.
14
15
16
17
18
19
20
21
22
23

24 **3.5 Application to a case study**

26 To show the applicability of the proposed model in real situations, a case study has been chosen. The case
27 study is a 18th century historical building (built from 1733–1743) designed by the Architect Luigi Vanvitelli on
28 an artificial island as a quarantine station for the port town of Ancona called “Mole Vanvitelliana”. During the
29 last two centuries, the building has taken different functions: in 1860 as a military citadel, then in 1884 a sugar
30 refinery. Now it is used as a site of a museum, as well as home for various exhibitions. The “Mole
31 Vanvitelliana” main building is rounded by a town-wall. Both the building walls and the town-wall are made
32 with the same type of mortar and bricks. Town-walls are strongly inclined, then the rain can wet the surfaces.
33 It is possible to observe a diffuse biodeterioration process (Figure 3). On the contrary, the facades of the
34 building are vertical and protected by the rain, then not characterized by bio-deterioration.
35
36
37
38
39
40
41

42 Two different datasets of images were collected. Firstly, DI extracted from video surveillance HD cameras were
43 collected, to check the applicability of the proposed model to images coming from this type of data source.
44 Then detailed images of the brick facades were manually collected with a HQ resolution camera. All the
45 images were resized [89], [90] to the same dimension (1780x1780) using the “imagemagick” tool, rel.7.1.1-
46 20 and cropped to obtain 773 256x256 sub-images coming from video surveillance cameras and 245 256x256
47 px images coming from HD cameras. The trained model was iteratively used to check its recognition ability in
48 a real case. Finally, the “accuracy” (number of correct predictions in respect to the number of images) has
49 been computed.
50
51
52
53
54
55
56
57

58 **4. RESULTS AND DISCUSSION**

59 **4.1 Evolution of the microalgae bio-deterioration process**

60
61
62
63
64
65

1
2
3
4
5
6
7
8
9
10
11
12
13
14
15
16
17
18
19
20
21
22
23
24
25
26
27
28
29
30
31
32
33
34
35
36
37
38
39
40
41
42
43
44
45
46
47
48
49
50
51
52
53
54
55
56
57
58
59
60
61
62
63
64
65

Figure 4a and Figure 4b shows, respectively, DI and RGB spectrum of the brick's samples (one for each type) before the inoculation (addiction of microalgae spores). Bricks are different by color: B sample is a dark-red brick with the lowest [RGB] spectrum values; AH and AL are light-red bricks with intermediate green [G] spectrum values and high red [R] values; finally, CH and CL are yellow bricks characterized by the highest [RGB] spectrum values.

As can be seen in Figure 5a, microalgae growth initially causes the comparison of little dark green spots (2), then the spots create more large green areas interconnecting with each other (3). These areas assume a typical shape, with largest spots and "filamentous" areas due to the water drainage. In the last phase microalgae growth cause the comparison of light green spots over the initial dark-green spots (4). The shape and the color of these spots and areas can be different depending on the brick's surface characteristics, the growth's phase, and the environmental conditions (Figure 5b).

Figure 6 shows the variation of CIELab mean values (DE) of the brick's surfaces during the experimental activity. Each curve represents the mean values of 27 measurement points (9 points x 3 samples). It is possible to observe a progressive increase of the DE values. DE reached 45-55 values for CH and CL samples after 35 days, 30-35 values for B (after 65 days), and 30-40 values for AH and AL (after 112 days) due to the microalgae coverage. A slight reduction of the peak values has been observed for samples AH and AL after 133 days. Considering that just DE values ≥ 2 are clearly perceived by the human eye, the color variation is very relevant, reaching a peak of 65 (CL) and confirming the observations made with the DI (Figure 5b).

4.2 CNN training and test

To identify the starts of the microalgae growth process, a CNN has been trained, tested and validated. Figure 7 shows the plot of the history training and test process. At the end of each epoch (iteration on the whole dataset) the accuracy with the "training" dataset and with the "test" dataset has been plotted. The final accuracy (ratio of the number of correct predictions to the total number of predictions made by the model) is 0.83, then 83% of the images with or without microalgae were correctly recognized.

4.3 Automatic identification of microalgae biodeterioration in a case study

To show the applicability of the proposed model, a case study has been selected. The case study is a historical building where security HD cameras are installed, then DI are constantly collected. Moreover, high resolution images are periodically collected during events, due to the public character of the building. DI coming from security cameras nearby the case study were "cropped" to 256x256. The trained CNN was then used to predict microalgae on these images. The application of the trained CNN to this group of images shows that the ability recognition of microalgae on the bricks' surfaces using DI collected through HD security cameras is affected by several factors. Slicing images coming from cameras gives low resolution sub-images, affecting the recognition ability. The accuracy calculated summing the correct predictions over the total number of

1 predictions il low (0.52) if compared to the accuracy calculated on the images of the test dataset (0.83).
2 Moreover, the DI acquired from these cameras includes other elements (ground, roads, roofs, etc.) that were
3 not part of the original dataset. When objects different from the bricks are included in the “cropped” image,
4 CNN frequently fails, reducing total accuracy. Then images with higher resolution are necessary. Moreover, it
5 is necessary to extend the dataset we used to train the CNN also with images including not only the bricks,
6 but also all the elements that it is possible to find on building facades and in the surrounding (Figure 8).

7
8
9
10 A second group of images directly collected near the building facades and including only bricks with and
11 without microalgae were acquired using an HD camera. Images were resized to 1780x1780 px and cropped
12 to 256x256 px to check the accuracy of the CNN (Figure 9).

13
14
15 In that case, accuracy increases reaching 0.68 value, but remaining lower than the accuracy found at the end
16 of the training ant test procedure (0.83). Then the increase of the resolution combined with the exclusion of
17 elements different than bricks improved recognition ability of the trained CNN. However, the not perfect
18 matching among the colors of the bricks used to train the CNN and the color of the historical bricks in the
19 case study and probably also the presence of other types of bio-colonizers and/or stains reduced the accuracy
20 obtained with real images. It is important to underline that no filtering actions were performed on images to
21 check the capability of the trained and tested CNN to work directly with real images.

22 23 24 25 26 27 28 29 30 **5. CONCLUSIONS**

31 Built cultural heritage is exposed to various deterioration problems that can be caused by different types of
32 actions. To reduce major invasive interventions, a “preventive conservation” approach was proposed, that
33 means a shift from restoration, intended as those activities needed to repair serious deteriorations, to a more
34 inclusive approach, based on a continuous care and supported by data collection, regular monitoring,
35 inspections, control of environmental factors and maintenance activities. Data collection and monitoring
36 actions are a fundamental part of a preventive conservation approach giving the possibility to realize “early”
37 damage detection systems. DI of historical buildings facades (constantly collected by different subjects and
38 for different purposes) represent the biggest available data source to support this approach and can be used
39 to develop predictive tools thanks to the advancements of artificial intelligence methods. This work was
40 addressed to the development of predictive models based on CNN to support a preventive conservation
41 approach. DI of historical façades were used to train a CNN able to recognize bio-colonization phenomena
42 by microalgae on bricks surfaces of historical buildings. The CNN has been trained and tested with images
43 collected during experimental activities. Five different types of bricks were subjected to a bio-colonization
44 process by microalgae and the chromatic alteration of the surface was detected during the growth process.
45 Experimental activities comprised a set of different environmental conditions.

46
47
48
49
50
51
52
53
54
55
56
57
58
59
60
61
62
63
64
65
66
67
68
69
70
71
72
73
74
75
76
77
78
79
80
81
82
83
84
85
86
87
88
89
90
91
92
93
94
95
96
97
98
99
100
101
102
103
104
105
106
107
108
109
110
111
112
113
114
115
116
117
118
119
120
121
122
123
124
125
126
127
128
129
130
131
132
133
134
135
136
137
138
139
140
141
142
143
144
145
146
147
148
149
150
151
152
153
154
155
156
157
158
159
160
161
162
163
164
165
166
167
168
169
170
171
172
173
174
175
176
177
178
179
180
181
182
183
184
185
186
187
188
189
190
191
192
193
194
195
196
197
198
199
200
201
202
203
204
205
206
207
208
209
210
211
212
213
214
215
216
217
218
219
220
221
222
223
224
225
226
227
228
229
230
231
232
233
234
235
236
237
238
239
240
241
242
243
244
245
246
247
248
249
250
251
252
253
254
255
256
257
258
259
260
261
262
263
264
265
266
267
268
269
270
271
272
273
274
275
276
277
278
279
280
281
282
283
284
285
286
287
288
289
290
291
292
293
294
295
296
297
298
299
300
301
302
303
304
305
306
307
308
309
310
311
312
313
314
315
316
317
318
319
320
321
322
323
324
325
326
327
328
329
330
331
332
333
334
335
336
337
338
339
340
341
342
343
344
345
346
347
348
349
350
351
352
353
354
355
356
357
358
359
360
361
362
363
364
365
366
367
368
369
370
371
372
373
374
375
376
377
378
379
380
381
382
383
384
385
386
387
388
389
390
391
392
393
394
395
396
397
398
399
400
401
402
403
404
405
406
407
408
409
410
411
412
413
414
415
416
417
418
419
420
421
422
423
424
425
426
427
428
429
430
431
432
433
434
435
436
437
438
439
440
441
442
443
444
445
446
447
448
449
450
451
452
453
454
455
456
457
458
459
460
461
462
463
464
465
466
467
468
469
470
471
472
473
474
475
476
477
478
479
480
481
482
483
484
485
486
487
488
489
490
491
492
493
494
495
496
497
498
499
500
501
502
503
504
505
506
507
508
509
510
511
512
513
514
515
516
517
518
519
520
521
522
523
524
525
526
527
528
529
530
531
532
533
534
535
536
537
538
539
540
541
542
543
544
545
546
547
548
549
550
551
552
553
554
555
556
557
558
559
560
561
562
563
564
565
566
567
568
569
570
571
572
573
574
575
576
577
578
579
580
581
582
583
584
585
586
587
588
589
590
591
592
593
594
595
596
597
598
599
600
601
602
603
604
605
606
607
608
609
610
611
612
613
614
615
616
617
618
619
620
621
622
623
624
625
626
627
628
629
630
631
632
633
634
635
636
637
638
639
640
641
642
643
644
645
646
647
648
649
650
651
652
653
654
655
656
657
658
659
660
661
662
663
664
665
666
667
668
669
670
671
672
673
674
675
676
677
678
679
680
681
682
683
684
685
686
687
688
689
690
691
692
693
694
695
696
697
698
699
700
701
702
703
704
705
706
707
708
709
710
711
712
713
714
715
716
717
718
719
720
721
722
723
724
725
726
727
728
729
730
731
732
733
734
735
736
737
738
739
740
741
742
743
744
745
746
747
748
749
750
751
752
753
754
755
756
757
758
759
760
761
762
763
764
765
766
767
768
769
770
771
772
773
774
775
776
777
778
779
780
781
782
783
784
785
786
787
788
789
790
791
792
793
794
795
796
797
798
799
800
801
802
803
804
805
806
807
808
809
810
811
812
813
814
815
816
817
818
819
820
821
822
823
824
825
826
827
828
829
830
831
832
833
834
835
836
837
838
839
840
841
842
843
844
845
846
847
848
849
850
851
852
853
854
855
856
857
858
859
860
861
862
863
864
865
866
867
868
869
870
871
872
873
874
875
876
877
878
879
880
881
882
883
884
885
886
887
888
889
890
891
892
893
894
895
896
897
898
899
900
901
902
903
904
905
906
907
908
909
910
911
912
913
914
915
916
917
918
919
920
921
922
923
924
925
926
927
928
929
930
931
932
933
934
935
936
937
938
939
940
941
942
943
944
945
946
947
948
949
950
951
952
953
954
955
956
957
958
959
960
961
962
963
964
965
966
967
968
969
970
971
972
973
974
975
976
977
978
979
980
981
982
983
984
985
986
987
988
989
990
991
992
993
994
995
996
997
998
999
1000

1 and test a CNN. The trained model is characterized by an accuracy of 83% and can recognize the starts of the
2 bio-colonization process on different types of bricks. The model has been then applied to a case study to
3 evaluate the ability of the model to recognize microalgae on historical bricks when DI extracted from video
4 surveillance HD cameras and/or HQ DI freely collected are available, as in the case of the case-study. Results
5 shows that the ability for the trained CNN to recognize microalgae on the bricks' surfaces using DI collected
6 through HD security cameras is affected by two main factors. Images extracted from video-surveillance
7 cameras are characterized by medium-low resolution, are captured not orthogonally to the walls and with
8 different illuminance conditions. These aspects affect the recognition ability of the trained CNN, lowering
9 accuracy. On the other side, acquired DI includes other elements (ground, roads, roofs, etc.) that were not
10 part of the original dataset. When objects different from the bricks are included in the "cropped" image, CNN
11 frequently fails. The use of high-resolution images collected on the case study including only bricks facades
12 increases accuracy. An accuracy value of 0.68 was obtained, then lower than the accuracy obtained with the
13 dataset of experimental images. It is important to underline that no-filtering actions were performed on the
14 captured images to check the ability of the CNN to work directly with real images. To overcome the main
15 limit underlined will be necessary to extend this study, increasing the dataset created with experimental
16 activities and including real case images representing all the elements that it is possible to find on building
17 facades and in the surroundings, and images representing different type of bio-colonizers. Despite the
18 declared limitations the proposed model is applicable to real cases to the early detection of microalgae bio-
19 colonization when DI of the details of bricks surfaces are collected.
20
21
22
23
24
25
26
27
28
29
30
31
32
33
34

35 6. ACKNOWLEDGEMENTS

36 This research did not receive any specific grant from funding agencies in the public, commercial, or not-for-
37 profit sectors.
38
39
40
41

42 REFERENCES

- 43
44
45 [1] J. Sanetra-Szeliga, *Cultural Heritage Counts for Europe: full report*. 2015. [Online]. Available:
46 [http://blogs.encatc.org/culturalheritagecountsforeurope//wp-](http://blogs.encatc.org/culturalheritagecountsforeurope//wp-content/uploads/2015/06/CHCfE_FULL-REPORT_v2.pdf)
47 [content/uploads/2015/06/CHCfE_FULL-REPORT_v2.pdf](http://blogs.encatc.org/culturalheritagecountsforeurope//wp-content/uploads/2015/06/CHCfE_FULL-REPORT_v2.pdf)
48
49
50 [2] E. Eken, B. Taşçı, and C. Gustafsson, "An evaluation of decision-making process on maintenance of
51 built cultural heritage: The case of Visby, Sweden," *Cities*, vol. 94, pp. 24–32, 2019, doi:
52 10.1016/j.cities.2019.05.030.
53
54 [3] ICOMOS, "ICOMOS Charter – Principles for the Analysis, Conservation and Structural Restoration of
55 Heritage, Architectural." 2003. [Online]. Available: [https://www.icomos.org/en/about-the-](https://www.icomos.org/en/about-the-centre/179-articles-en-francais/ressources/charters-and-standards/165-icomos-charter-principles-)
56 [centre/179-articles-en-francais/ressources/charters-and-standards/165-icomos-charter-principles-](https://www.icomos.org/en/about-the-centre/179-articles-en-francais/ressources/charters-and-standards/165-icomos-charter-principles-)
57
58
59
60
61
62
63
64
65

for-the-analysis-conservation-and-structural-restoration-of-architectural-heritage

- [4] K. Van Balen, "Preventive Conservation of Historic Buildings," *Restor. Build. Monum.*, vol. 21, no. 2–3, pp. 99–104, 2015, doi: 10.1515/rbm-2015-0008.
- [5] S. Della Torre, "Italian perspective on the planned preventive conservation of architectural heritage," *Front. Archit. Res.*, vol. 10, no. 1, pp. 108–116, 2021, doi: 10.1016/j.foar.2020.07.008.
- [6] J. Sroczyńska, "Preventive maintenance of historical buildings in European countries," vol. 2, no. 70, pp. 51–57, 2022, doi: 10.37190/arc220205.
- [7] P. B. Lourenço, A. Barontini, D. V. Oliveira, and J. Ortega, "Rethinking preventive conservation: Recent examples," in *Geotechnical Engineering for the Preservation of Monuments and Historic Sites III - Proc. 3rd International Symposium on Geotechnical Engineering for the Preservation of Monuments and Historic Sites – TC301 – IS, Napoli, 22-24 June 2022*, London: CRC Press, 2022, pp. 70–86. doi: 10.1201/9781003308867-4.
- [8] G. Caneva, M. P. Nugari, O. Salvadori, and ICCROM - International Centre for the Study of the Preservation and the Restoration of Cultural Property, *Biology in the Conservation of Works of Art*. Roma: Sintesi Grafica Srl, 1991.
- [9] H. Barberousse, B. Ruot, C. Yéprémian, and G. Boulon, "An assessment of façade coatings against colonisation by aerial algae and cyanobacteria," *Build. Environ.*, vol. 42, no. 7, pp. 2555–2561, Jul. 2007, doi: 10.1016/j.buildenv.2006.07.031.
- [10] M. L. Coutinho, A. Z. Miller, and M. F. Macedo, "Biological colonization and biodeterioration of architectural ceramic materials : An overview," *J. Cult. Herit.*, vol. 16, no. 5, pp. 759–777, 2015, doi: 10.1016/j.culher.2015.01.006.
- [11] C. C. Gaylarde and P. M. Gaylarde, "A comparative study of the major microbial biomass of biofilms on exteriors of buildings in Europe and Latin America," *Int. Biodeterior. Biodegradation*, vol. 55, pp. 131–139, 2005, doi: 10.1016/j.ibiod.2004.10.001.
- [12] C. Gaylarde, M. Ribas Silva, and T. Warscheid, "Microbial impact on building materials: an overview," *Mater. Struct.*, vol. 36, no. 5, pp. 342–352, 2003, doi: 10.1007/bf02480875.
- [13] V. P. de F. I. Flores-Colen, J. de Brito, "Stains in facades' rendering – Diagnosis and maintenance techniques' classification," vol. 22, pp. 211–221, 2008, doi: 10.1016/j.conbuildmat.2006.08.023.
- [14] S. Sannigrahi, F. Pilla, B. Basu, A. S. Basu, and A. Molter, "Examining the association between socio-demographic composition and COVID-19 fatalities in the European region using spatial regression approach," *Sustain. Cities Soc.*, vol. 62, no. July, p. 102418, 2020, doi: 10.1016/j.scs.2020.102418.
- [15] G. Caneva, F. Bartoli, M. Fontani, D. Mazzeschi, and P. Visca, "Changes in biodeterioration patterns of mural paintings: Multi-temporal mapping for a preventive conservation strategy in the Crypt of the Original Sin (Matera, Italy)," *J. Cult. Herit.*, vol. 40, pp. 59–68, 2019, doi: 10.1016/j.culher.2019.05.011.

- 1
2
3
4
5
6
7
8
9
10
11
12
13
14
15
16
17
18
19
20
21
22
23
24
25
26
27
28
29
30
31
32
33
34
35
36
37
38
39
40
41
42
43
44
45
46
47
48
49
50
51
52
53
54
55
56
57
58
59
60
61
62
63
64
65
- [16] R. Douglas-Jones, J. J. Hughes, S. Jones, and T. Yarrow, "Science, value and material decay in the conservation of historic environments," *J. Cult. Herit.*, vol. 21, pp. 823–833, 2016, doi: 10.1016/j.culher.2016.03.007.
- [17] E. Quagliarini, B. Gregorini, and M. D’Orazio, "Modelling microalgae biofouling on porous buildings materials: a novel approach," *Mater. Struct. Constr.*, vol. 55, no. 6, Jul. 2022, doi: 10.1617/s11527-022-01993-x.
- [18] O. Guillitte, "Bioreceptivity: a new concept for building ecology studies," *Sci. Total Environ.*, vol. 167, no. 1–3, pp. 215–220, 1995, doi: 10.1016/0048-9697(95)04582-L.
- [19] T. Warscheid and J. Braams, "Biodeterioration of stone: A review," *Int. Biodeterior. Biodegrad.*, vol. 46, no. 4, pp. 343–368, 2000, doi: 10.1016/S0964-8305(00)00109-8.
- [20] L. Tomaselli, G. Lamenti, M. Bosco, and P. Tiano, "Biodiversity of photosynthetic micro-organisms dwelling on stone monuments," *Int. Biodeterior. Biodegrad.*, vol. 46, no. 3, pp. 251–258, 2000, doi: 10.1016/S0964-8305(00)00078-0.
- [21] M. L. Coutinho, A. Z. Miller, and M. F. Macedo, "Biological colonization and biodeterioration of architectural ceramic materials: An overview," *Journal of Cultural Heritage*, vol. 16, no. 5. Elsevier Masson SAS, pp. 759–777, Sep. 01, 2015. doi: 10.1016/j.culher.2015.01.006.
- [22] C. Gaylarde, M. Ribas Silva, and T. Warscheid, "Microbial impact on building materials: an overview," *Mater. Struct.*, vol. 36, no. 5, pp. 342–352, 2003, doi: 10.1007/bf02480875.
- [23] C. C. Gaylarde and P. M. Gaylarde, "A comparative study of the major microbial biomass of biofilms on exteriors of buildings in Europe and Latin America," *Int. Biodeterior. Biodegrad.*, vol. 55, no. 2, pp. 131–139, 2005, doi: 10.1016/j.ibiod.2004.10.001.
- [24] F. C. Carniel *et al.*, "New features of desiccation tolerance in the lichen photobiont *Trebouxia gelatinosa* are revealed by a transcriptomic approach," *Plant Mol. Biol.*, vol. 91, no. 3, pp. 319–339, 2016, doi: 10.1007/s11103-016-0468-5.
- [25] L. Graziani, E. Quagliarini, A. Osimani, L. Aquilanti, F. Clementi, and M. D’Orazio, "The influence of clay brick substratum on the inhibitory efficiency of TiO₂ nanocoating against biofouling," *Build. Environ.*, vol. 82, pp. 128–134, 2014, doi: 10.1016/j.buildenv.2014.08.013.
- [26] L. Graziani, E. Quagliarini, and M. D’Orazio, "The role of roughness and porosity on the self-cleaning and anti-biofouling efficiency of TiO₂-Cu and TiO₂-Ag nanocoatings applied on fired bricks," *Constr. Build. Mater.*, vol. 129, 2016, doi: 10.1016/j.conbuildmat.2016.10.111.
- [27] T. H. Tran *et al.*, "Influence of the intrinsic characteristics of mortars on biofouling by *Klebsormidium flaccidum*," *Int. Biodeterior. Biodegradation*, vol. 70, pp. 31–39, 2012, doi: 10.1016/J.IBIOD.2011.10.017.
- [28] H. S. Munawar, A. W. A. Hammad, A. Haddad, C. A. P. Soares, and S. T. Waller, "Image-based crack detection methods: A review," *Infrastructures*, vol. 6, no. 8. MDPI AG, Aug. 01, 2021. doi:

10.3390/infrastructures6080115.

- 1
2 [29] J. Valença, E. N. Brito Santos Júlio, and H. J. Araujo, "Intelligent Concrete Health Monitoring (ICHM):
3 An Innovative Method for Monitoring Concrete Structures using Multi Spectral Analysis and Image
4 Processing," in *8th fib PhD Symposium in Kgs. Lyngby, Denmark, June 20-23, 2010*.
- 5
6 [30] B. O. Santos, J. Valença, and E. Júlio, "Detection of cracks on concrete surfaces by hyperspectral
7 image processing," in *Proc. of Automated Visual Inspection and Machine Vision II, 25-29 June,*
8 *Munich, Germany, 2017*, vol. 10334, pp. 1033407–1/19. doi: 10.1117/12.2269606.
- 9
10 [31] J. Valença, D. Dias-Da-Costa, and E. N. B.S. Júlio, "Characterisation of concrete cracking during
11 laboratorial tests using image processing," *Construction and Building Materials*, vol. 28, no. 1. pp.
12 607–615, 2012. doi: 10.1016/j.conbuildmat.2011.08.082.
- 13
14 [32] J. Valença, D. Dias-Da-Costa, E. Júlio, H. Araújo, and H. Costa, "Automatic crack monitoring using
15 photogrammetry and image processing," *Meas. J. Int. Meas. Confed.*, vol. 46, no. 1, pp. 433–441,
16 2013, doi: 10.1016/j.measurement.2012.07.019.
- 17
18 [33] B. Kim and S. Cho, "Automated vision-based detection of cracks on concrete surfaces using a deep
19 learning technique," *Sensors (Switzerland)*, vol. 18, no. 10, Oct. 2018, doi: 10.3390/s18103452.
- 20
21 [34] R. Li, J. Yu, F. Li, R. Yang, Y. Wang, and Z. Peng, "Automatic bridge crack detection using Unmanned
22 aerial vehicle and Faster R-CNN," *Constr. Build. Mater.*, vol. 362, 2023, doi:
23 10.1016/j.conbuildmat.2022.129659.
- 24
25 [35] H. Wan *et al.*, "A novel transformer model for surface damage detection and cognition of concrete
26 bridges," *Expert Syst. Appl.*, vol. 213, p. 119019, Mar. 2023, doi: 10.1016/j.eswa.2022.119019.
- 27
28 [36] V. Vivekananthan, R. Vignesh, S. Vasanthaseelan, E. Joel, and K. S. Kumar, "Concrete bridge crack
29 detection by image processing technique by using the improved OTSU method," *Mater. Today Proc.*,
30 vol. 74, pp. 1002–1007, Jan. 2023, doi: 10.1016/j.matpr.2022.11.356.
- 31
32 [37] J. Zhang, S. Qian, and C. Tan, "Automated bridge surface crack detection and segmentation using
33 computer vision-based deep learning model," *Eng. Appl. Artif. Intell.*, vol. 115, Oct. 2022, doi:
34 10.1016/j.engappai.2022.105225.
- 35
36 [38] K. Jang, H. Jung, and Y. K. An, "Automated bridge crack evaluation through deep super resolution
37 network-based hybrid image matching," *Autom. Constr.*, vol. 137, 2022, doi:
38 10.1016/j.autcon.2022.104229.
- 39
40 [39] J. Valença, I. Puente, E. Júlio, H. González-Jorge, and P. Arias-Sánchez, "Assessment of cracks on
41 concrete bridges using image processing supported by laser scanning survey," *Constr. Build. Mater.*,
42 vol. 146, pp. 668–678, Aug. 2017, doi: 10.1016/j.conbuildmat.2017.04.096.
- 43
44 [40] W. W. Jin *et al.*, "Road Pavement Damage Detection Based on Local Minimum of Grayscale and
45 Feature Fusion," *Appl. Sci.*, vol. 12, no. 24, Dec. 2022, doi: 10.3390/app122413006.
- 46
47 [41] M. Abdellatif, H. Peel, A. G. Cohn, and R. Fuentes, "Pavement crack detection from hyperspectral
48
49
50
51
52
53
54
55
56
57
58
59
60
61
62
63
64
65

images using a novel asphalt crack index," *Remote Sens.*, vol. 12, no. 18, Sep. 2020, doi:
10.3390/RS12183084.

- [42] K. Lu, "Advances in deep learning methods for pavement surface crack detection," in *Proc. Conf. Computer Vision and Pattern Recognition, Virtual, 14-19 June, 2020*. doi:
<https://doi.org/10.48550/arXiv.2012.14704>.
- [43] L. Zhang, F. Yang, Y. Daniel Zhang, and Y. J. Zhu, "Road crack detection using deep convolutional neural network," *Proc. - Int. Conf. Image Process. ICIP*, pp. 3708–3712, 2016, doi:
10.1109/ICIP.2016.7533052.
- [44] A. Rezaie, R. Achanta, M. Godio, and K. Beyer, "Comparison of crack segmentation using digital image correlation measurements and deep learning," *Constr. Build. Mater.*, vol. 261, Nov. 2020, doi:
10.1016/j.conbuildmat.2020.120474.
- [45] L. Minh Dang *et al.*, "Deep learning-based masonry crack segmentation and real-life crack length measurement," *Constr. Build. Mater.*, vol. 359, 2022, doi: 10.1016/j.conbuildmat.2022.129438.
- [46] D. Loverdos and V. Sarhosis, "Automatic image-based brick segmentation and crack detection of masonry walls using machine learning," *Autom. Constr.*, vol. 140, Aug. 2022, doi:
10.1016/j.autcon.2022.104389.
- [47] N. Wang, Q. Zhao, S. Li, X. Zhao, and P. Zhao, "Damage Classification for Masonry Historic Structures Using Convolutional Neural Networks Based on Still Images," *Comput. Civ. Infrastruct. Eng.*, vol. 33, no. 12, pp. 1073–1089, Dec. 2018, doi: 10.1111/mice.12411.
- [48] N. Wang, X. Zhao, P. Zhao, Y. Zhang, Z. Zou, and J. Ou, "Automatic damage detection of historic masonry buildings based on mobile deep learning," *Autom. Constr.*, vol. 103, pp. 53–66, Jul. 2019, doi: 10.1016/j.autcon.2019.03.003.
- [49] N. Wang, X. Zhao, Z. Zou, P. Zhao, and F. Qi, "Autonomous damage segmentation and measurement of glazed tiles in historic buildings via deep learning," *Comput. Civ. Infrastruct. Eng.*, vol. 35, no. 3, pp. 277–291, Mar. 2020, doi: 10.1111/mice.12488.
- [50] Z. Zou, X. Zhao, P. Zhao, F. Qi, and N. Wang, "CNN-based statistics and location estimation of missing components in routine inspection of historic buildings," *J. Cult. Herit.*, vol. 38, pp. 221–230, Jul. 2019, doi: 10.1016/j.culher.2019.02.002.
- [51] A. L. C. Ottoni, R. M. De Amorim, M. S. Novo, and D. B. Costa, "Tuning of data augmentation hyperparameters in deep learning to building construction image classification with small datasets," *Int. J. Mach. Learn. Cybern.*, vol. 14, no. 1, pp. 171–186, 2023, doi: 10.1007/s13042-022-01555-1.
- [52] E. Hatır, M. Korkanç, A. Schachner, and İ. İnce, "The deep learning method applied to the detection and mapping of stone deterioration in open-air sanctuaries of the Hittite period in Anatolia," *J. Cult. Herit.*, vol. 51, pp. 37–49, Sep. 2021, doi: 10.1016/j.culher.2021.07.004.
- [53] J. W. R. Chong *et al.*, "Microalgae identification: Future of image processing and digital algorithm,"

Bioresour. Technol., vol. 369, no. November 2022, p. 128418, 2023, doi:

10.1016/j.biortech.2022.128418.

- [54] P. Otálora, J. L. Guzmán, F. G. Acién, M. Berenguel, and A. Reul, "Microalgae classification based on machine learning techniques," *Algal Res.*, vol. 55, no. February, 2021, doi: 10.1016/j.algal.2021.102256.
- [55] Z. Zhuo, H. Wang, R. Liao, and H. Ma, "Machine Learning Powered Microalgae Classification by Use of Polarized Light Scattering Data," *Appl. Sci.*, vol. 12, no. 7, 2022, doi: 10.3390/app12073422.
- [56] M. E. Sonmez, N. Eczacioglu, N. E. Gumuş, M. F. Aslan, K. Sabanci, and B. Aşikkutlu, "Convolutional neural network - Support vector machine based approach for classification of cyanobacteria and chlorophyta microalgae groups," *Algal Res.*, vol. 61, no. November 2021, 2022, doi: 10.1016/j.algal.2021.102568.
- [57] D. P. Yadav, A. S. Jalal, D. Garlapati, K. Hossain, A. Goyal, and G. Pant, "Deep learning-based ResNeXt model in phycological studies for future," *Algal Res.*, vol. 50, no. May, p. 102018, 2020, doi: 10.1016/j.algal.2020.102018.
- [58] G. Pant, D. P. Yadav, and A. Gaur, "ResNeXt convolution neural network topology-based deep learning model for identification and classification of *Pediastrum*," *Algal Res.*, vol. 48, no. May, p. 101932, 2020, doi: 10.1016/j.algal.2020.101932.
- [59] M. Kloster, D. Langenkämper, M. Zurowietz, B. Beszteri, and T. W. Nattkemper, "Deep learning-based diatom taxonomy on virtual slides," *Sci. Rep.*, vol. 10, no. 1, pp. 1–13, 2020, doi: 10.1038/s41598-020-71165-w.
- [60] G. Liu, S. Tian, G. Xu, C. Zhang, and M. Cai, "Combination of effective color information and machine learning for rapid prediction of soil water content," *J. Rock Mech. Geotech. Eng.*, Mar. 2023, doi: 10.1016/j.jrmge.2022.12.029.
- [61] J. Park, H. Lee, C. Y. Park, S. Hasan, T. Y. Heo, and W. H. Lee, "Algal morphological identification in watersheds for drinking water supply using neural architecture search for convolutional neural network," *Water (Switzerland)*, vol. 11, no. 7, 2019, doi: 10.3390/w11071338.
- [62] J. Park, J. Baek, J. Kim, K. You, and K. Kim, "Deep Learning-Based Algal Detection Model Development Considering Field Application," *Water (Switzerland)*, vol. 14, no. 8, pp. 1–14, 2022, doi: 10.3390/w14081275.
- [63] S. S. Baek *et al.*, "Identification and enumeration of cyanobacteria species using a deep neural network," *Ecol. Indic.*, vol. 115, no. April, p. 106395, 2020, doi: 10.1016/j.ecolind.2020.106395.
- [64] T. H. Tran and N. D. Hoang, "Estimation of algal colonization growth on mortar surface using a hybridization of machine learning and metaheuristic optimization," *Sadhana - Acad. Proc. Eng. Sci.*, vol. 42, no. 6, pp. 929–939, Jun. 2017, doi: 10.1007/s12046-017-0652-6.
- [65] T. H. Tran and N. D. Hoang, "Predicting algal appearance on mortar surface with ensembles of

adaptive neuro fuzzy models: a comparative study of ensemble strategies,” *Int. J. Mach. Learn. Cybern.*, vol. 10, no. 7, pp. 1687–1704, Jul. 2019, doi: 10.1007/s13042-018-0846-1.

- [66] J. Valença, L. M. S. Gonçalves, and E. N. B. S. Júlio, “Assessment of Concrete Surfaces Using Multi-Spectral Image Analysis,” in *35th Annual Symposium of IABSE / 52nd Annual Symposium of IASS / 6th International Conference on Space Structures: Taller, Longer, Lighter - Meeting growing demand with limited resources, London, United Kingdom, September, 2011*.
- [67] J. Valença, L. M. S. Gonçalves, and E. Júlio, “Damage assessment on concrete surfaces using multi-spectral image analysis,” *Constr. Build. Mater.*, vol. 40, pp. 971–981, Mar. 2013, doi: 10.1016/J.CONBUILDMAT.2012.11.061.
- [68] S. Bang, S. Park, H. Kim, and H. Kim, “Encoder–decoder network for pixel-level road crack detection in black-box images,” *Comput. Civ. Infrastruct. Eng.*, vol. 34, no. 8, pp. 713–727, 2019, doi: 10.1111/mice.12440.
- [69] “ASTM D4404-10. Standard test method for determination of pore volume and pore volume distribution of soil and rock by mercury intrusion porosimetry. American Society for Testing and Materials.” American Society for Testing and Materials, 2010.
- [70] *UNI EN ISO 4287:2009 - Geometrical Product Specifications (GPS) - Surface texture: Profile method - Terms, definitions and surface texture parameters*. International Standards Organization, 2009.
- [71] A. Dubosc, G. Escadeillas, and P. J. Blanc, “Characterization of biological stains on external concrete walls and influence of concrete as underlying material,” *Cem. Concr. Res.*, vol. 31, no. 11, pp. 1613–1617, 2001, doi: 10.1016/S0008-8846(01)00613-5.
- [72] L. Graziani *et al.*, “Evaluation of inhibitory effect of TiO₂ nanocoatings against microalgal growth on clay brick façades under weak UV exposure conditions,” *Build. Environ.*, vol. 64, pp. 38–45, Jun. 2013, doi: 10.1016/j.buildenv.2013.03.003.
- [73] “ASTM D5589-09. Standard test method for determining the resistance of paint films and related coatings to algal defacement. American Society for Testing and Materials.” 2009.
- [74] H. Barberousse, *Étude de la diversité des algues et des cyanobactéries colonisant les revêtements de façade en France et recherche des facteurs favorisant leur implantation*. 2006.
- [75] A. Dubosc, “Étude de développement de salissures biologiques sur les parements en béton: mise au point d’essais accélérés de vieillissement,” *Lab. Matériaux Durabilité des Constr.*, 2000.
- [76] “UNI EN ISO 12571:2013. Hygrothermal performance of building materials and products - Determination of hygroscopic sorption properties.” 2013.
- [77] H. W. Thorp, *Chemical Engineers’ Handbook. Second edition (Perry, John H., ed.)*, vol. 19, no. 9. 1942. doi: 10.1021/ed019p449.2.
- [78] L. Graziani, E. Quagliarini, and M. D’Orazio, “TiO₂-treated different fired brick surfaces for biofouling prevention: Experimental and modelling results,” *Ceram. Int.*, vol. 42, no. 3, pp. 4002–4010, Feb.

2016, doi: 10.1016/j.ceramint.2015.11.069.

- 1
2
3
4
5
6
7
8
9
10
11
12
13
14
15
16
17
18
19
20
21
22
23
24
25
26
27
28
29
30
31
32
33
34
35
36
37
38
39
40
41
42
43
44
45
46
47
48
49
50
51
52
53
54
55
56
57
58
59
60
61
62
63
64
65
- [79] O. Guillitte and R. Dreesen, "Laboratory chamber studies and petrographical analysis as bioreceptivity assessment tools of building materials," *Sci. Total Environ.*, vol. 167, no. 1–3, pp. 365–374, 1995, doi: 10.1016/0048-9697(95)04596-S.
- [80] G. Escadeillas, A. Bertron, E. Ringot, P. J. Blanc, and A. Dubosc, "Accelerated testing of biological stain growth on external concrete walls. Part 1: Quantification of growths," *Mater. Struct.*, vol. 42, no. 7, pp. 937–945, 2009, doi: 10.1617/s11527-008-9433-3.
- [81] A. Konopka and T. D. Brock, "Effect of Temperature on Blue-Green-Algae (Cyanobacteria) in Lake Mendota," *Appl. Environ. Microbiol.*, vol. 36, no. 4, pp. 572–576, 1978.
- [82] S. P. Singh and P. Singh, "Effect of temperature and light on the growth of algae species: A review," *Renew. Sustain. Energy Rev.*, vol. 50, pp. 431–444, 2015, doi: 10.1016/j.rser.2015.05.024.
- [83] R. Serra-Maia, O. Bernard, A. Gonçalves, S. Bensalem, and F. Lopes, "Influence of temperature on *Chlorella vulgaris* growth and mortality rates in a photobioreactor," *Algal Res.*, vol. 18, pp. 352–359, 2016, doi: 10.1016/j.algal.2016.06.016.
- [84] J. A. Raven and R. J. Geider, "Temperature and algal growth," *New Phytol.*, vol. 110, no. 4, pp. 441–461, 1988, doi: 10.1111/j.1469-8137.1988.tb00282.x.
- [85] K. Lengsfeld and M. Krus, "Microorganism on façades – reasons , consequences and measures," no. Venzmer, pp. 0–7, 2001.
- [86] J. Radulovic *et al.*, "Biofouling resistance and practical constraints of titanium dioxide nanoparticulate silane/siloxane exterior facade treatments," *Build. Environ.*, vol. 68, pp. 150–158, 2013, doi: 10.1016/j.buildenv.2013.07.001.
- [87] "UNI EN 15886:2010. Conservation of cultural property - Test methods - Colour measurement of surfaces," 2010.
- [88] "UNI 11721:2018. Materiali lapidei - Metodi di prova – Misurazione preventiva della variazione colorimetrica di superfici di pietra." 2018.
- [89] J. W. R. Chong *et al.*, "Microalgae identification: Future of image processing and digital algorithm," *Bioresource Technology*, vol. 369. Elsevier Ltd, Feb. 01, 2023. doi: 10.1016/j.biortech.2022.128418.
- [90] P. Otálora, J. L. Guzmán, F. G. Ación, M. Berenguel, and A. Reul, "Microalgae classification based on machine learning techniques," *Algal Res.*, vol. 55, May 2021, doi: 10.1016/j.algal.2021.102256.

FIGURE CAPTIONS

1
2
3 Figure 1. Research framework
4
5

6
7 Figure 2. Test apparatus for the evaluation of relative humidity influence on growth process (a) and for
8 accelerated test aimed at temperature effect investigation (b).
9

10
11
12 Figure 3. Mole Vanvitelliana, Ancona, Italy.
13
14

15
16 Figure 4. a) DI of brick's samples before the inoculation of algae spores. From left to right: AH, AL, B, CH, CL.
17 b) [RGB] spectrums of DI of brick's samples before the inoculation of algae spores. From upper to bottom:
18 AH, AL, B, CH, CL.
19
20
21

22
23 Figure 5. a) DI of the AL type brick during the microalgae growth process. 1: before microalgae inoculation;
24 2, 3, 4: after microalgae inoculation. b) Samples of collected DI of the different brick's types during the
25 microalgae growth process.
26
27

28
29 Figure 6. CIELab variation (DE) of brick's surfaces during microalgae growth process.
30
31

32
33 Figure 7. Plot of the "training and test" history process. The black line represents the accuracy obtained at
34 the end of each epoch during the training process. The red line represents the accuracy obtained at the end
35 of each epoch during the test process.
36
37
38

39
40 Figure 8. Images extracted from HS surveillance cameras and "cropped" to 256x256 px.
41
42

43
44 Figure 9. Images collected with cameras and "cropped" to 256x256.
45
46
47
48
49
50
51
52
53
54
55
56
57
58
59
60
61
62
63
64
65

TABLES

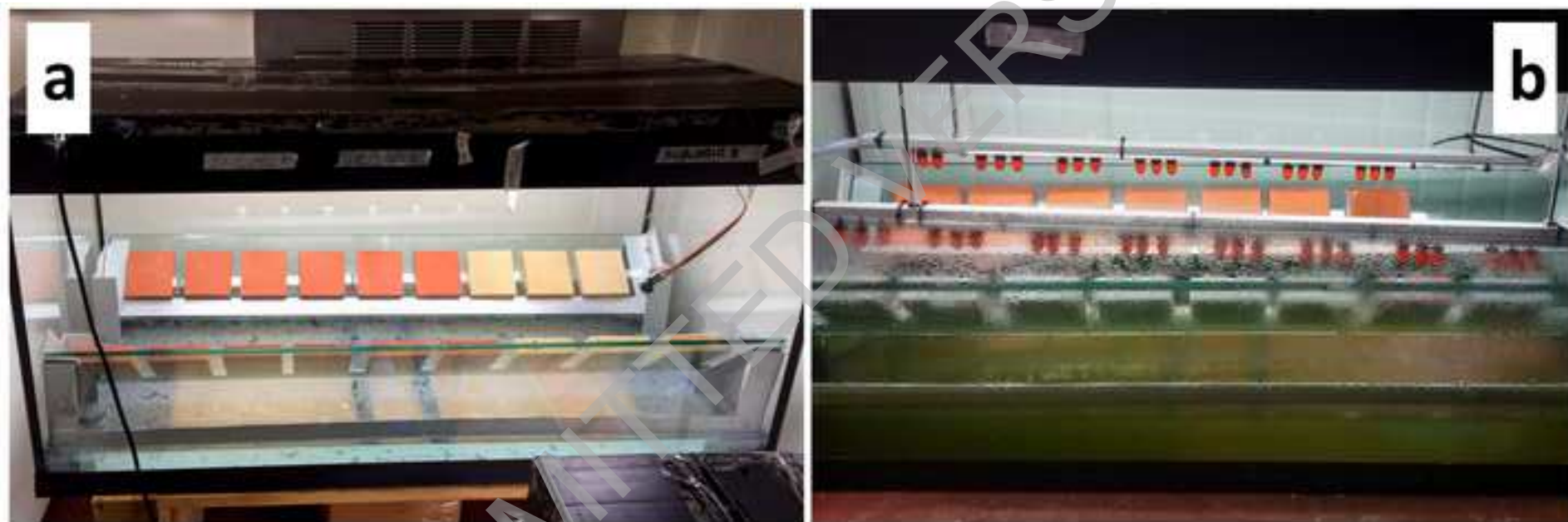
Table 1. Properties of the bricks used in the experimental activity.

Brick Type	Colour	Total porosity [%]	Roughness [μm]
AR	light-red	19.24 ± 0.37	5.54 ± 0.42
AS	light red	19.24 ± 0.37	4.50 ± 0.27
B	dark red	24.62 ± 1.02	2.95 ± 0.63
CR	yellow	44.09 ± 1.63	7.60 ± 0.57
CS	yellow	44.09 ± 1.63	6.60 ± 0.49

SUBMITTED VERSION

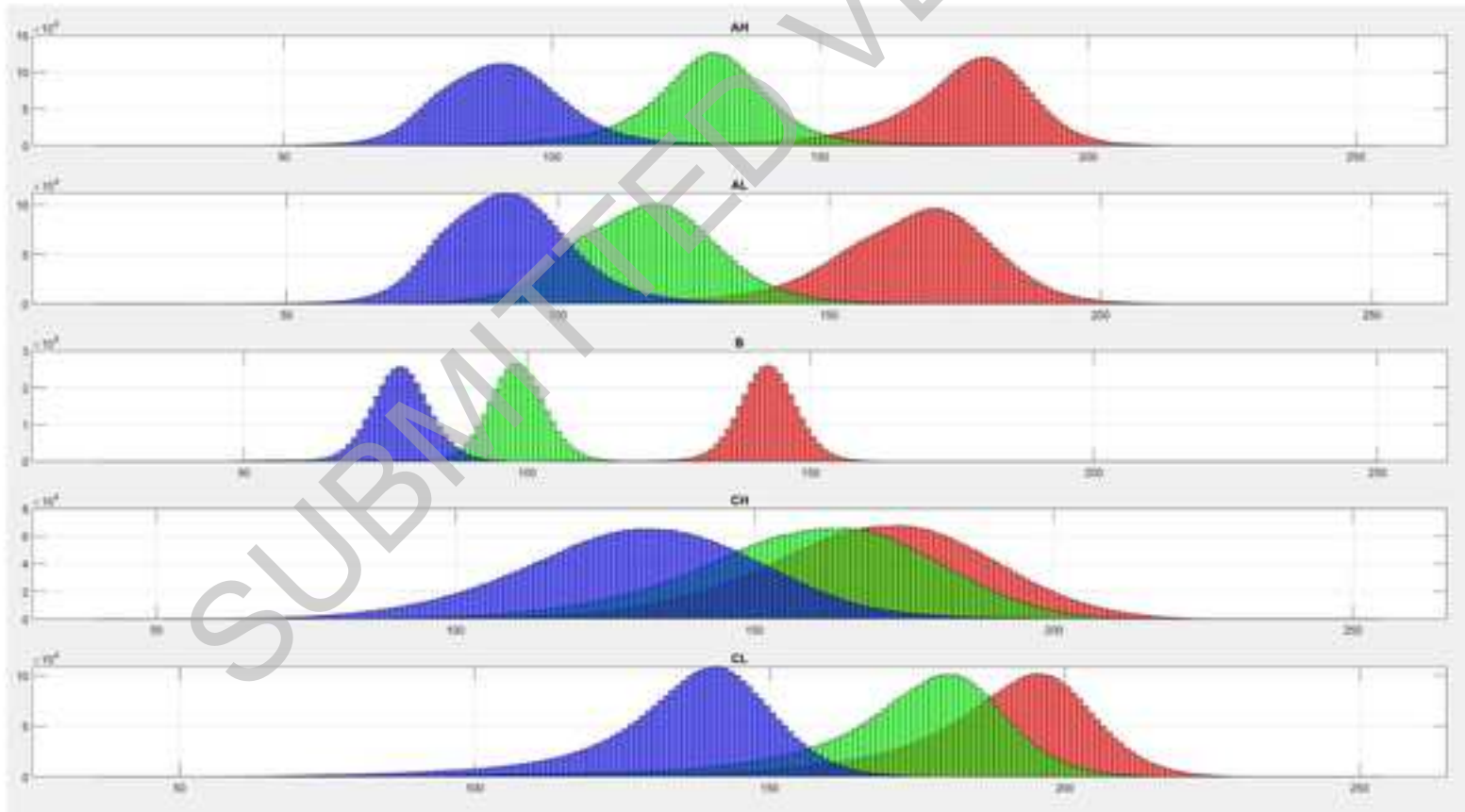
1
2
3
4
5
6
7
8
9
10
11
12
13
14
15
16
17
18
19
20
21
22
23
24
25
26
27
28
29
30
31
32
33
34
35
36
37
38
39
40
41
42
43
44
45
46
47
48
49
50
51
52
53
54
55
56
57
58
59
60
61
62
63
64
65

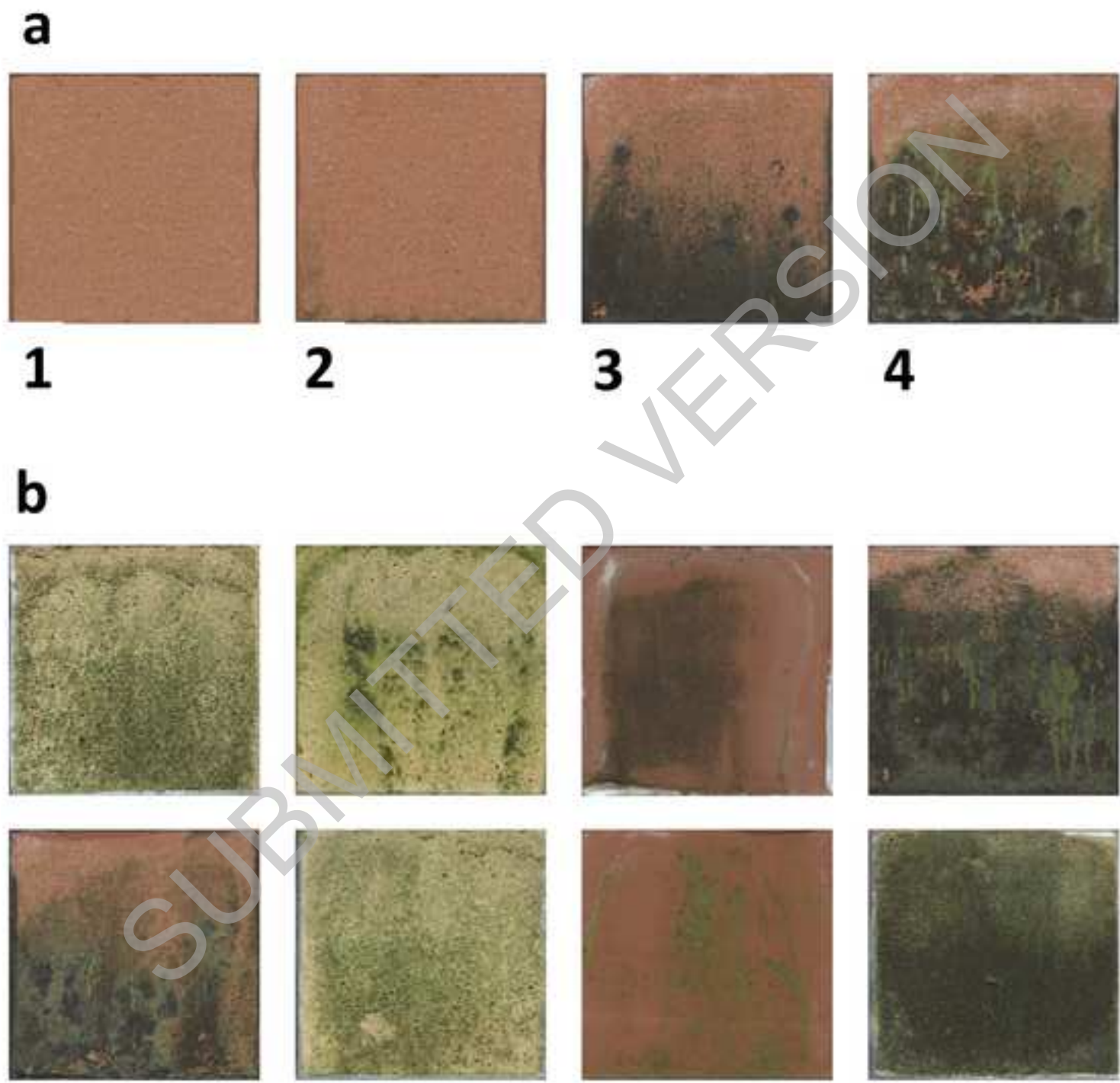






SUBMITTED VERSION

a**b**



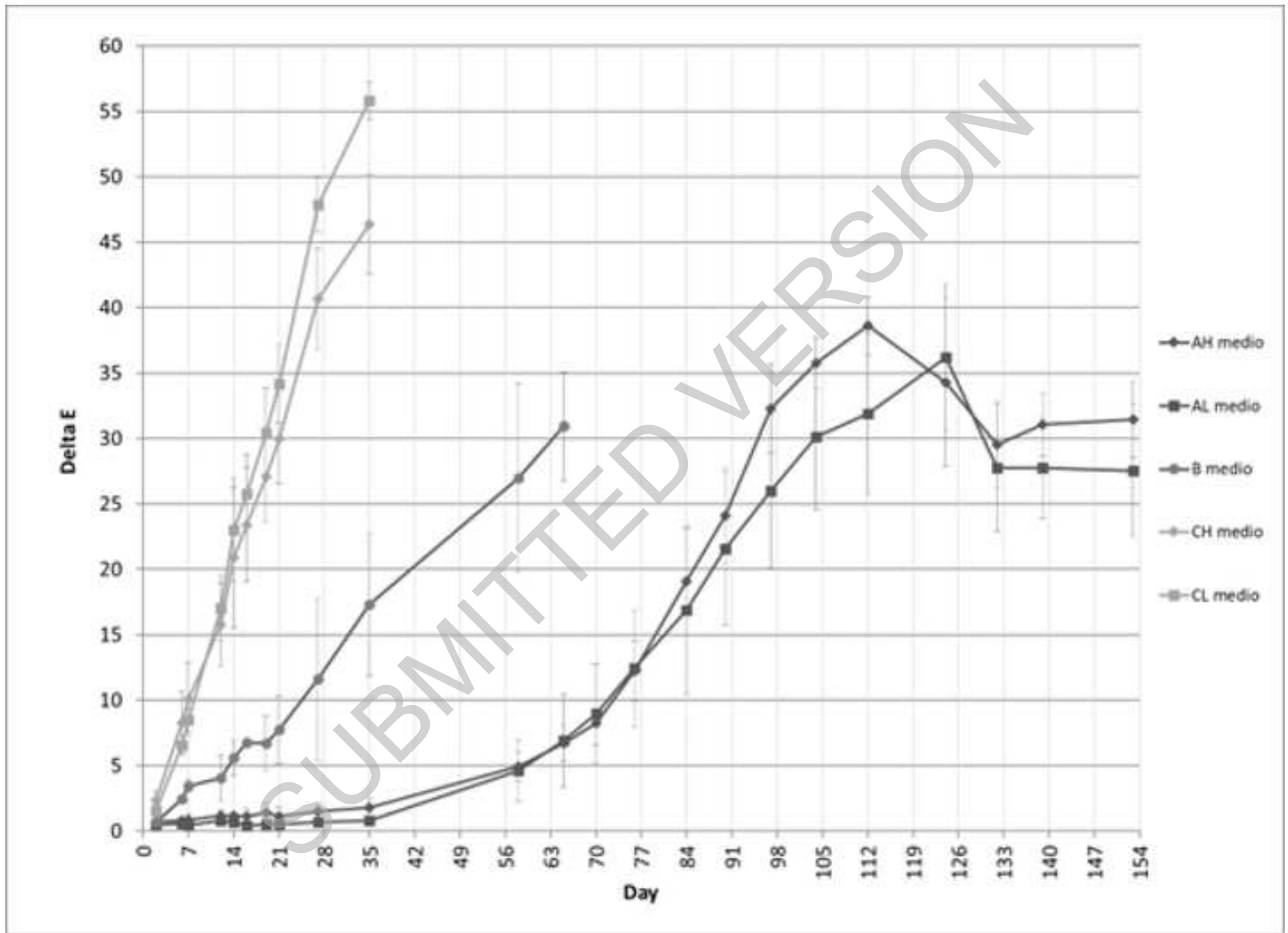
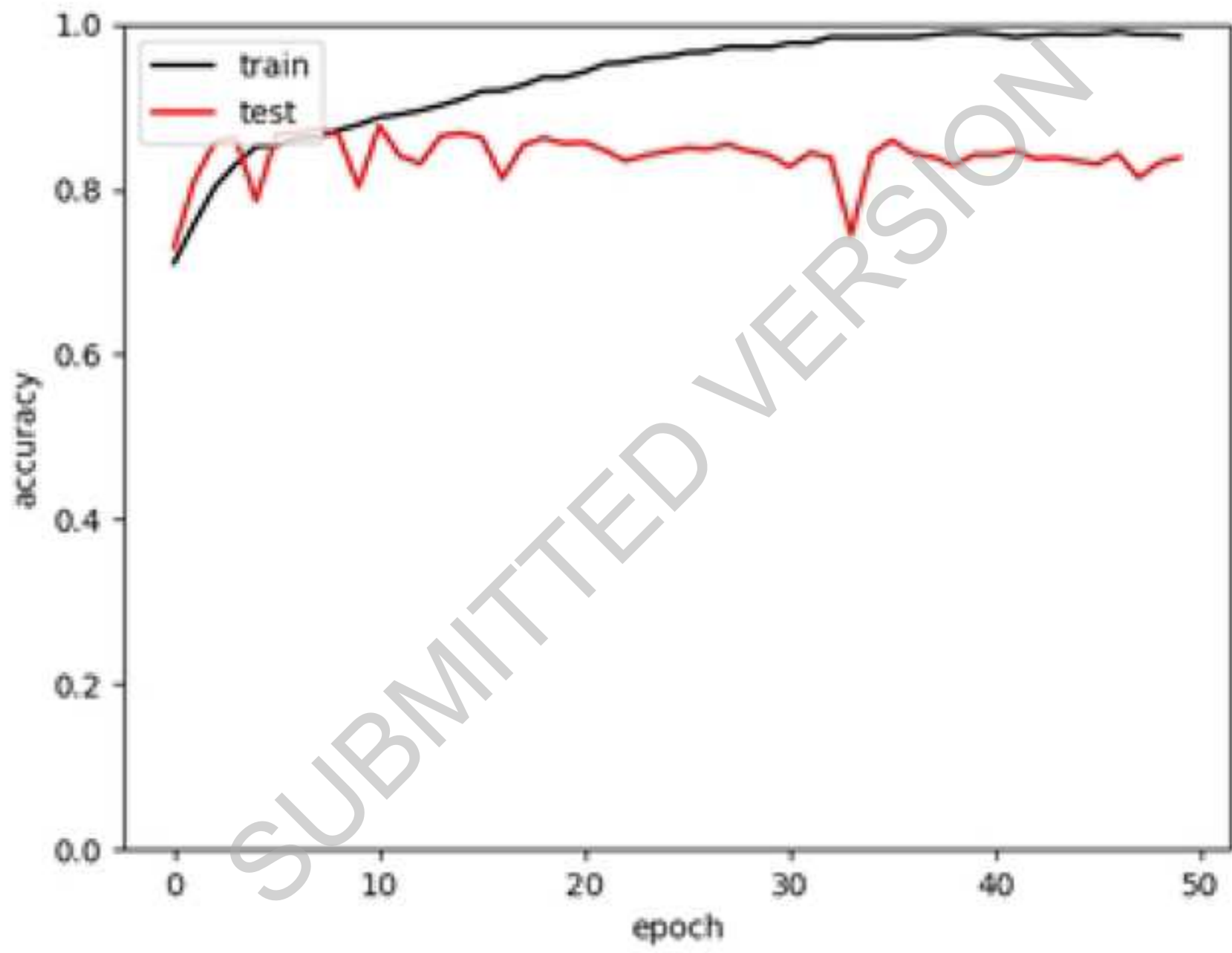
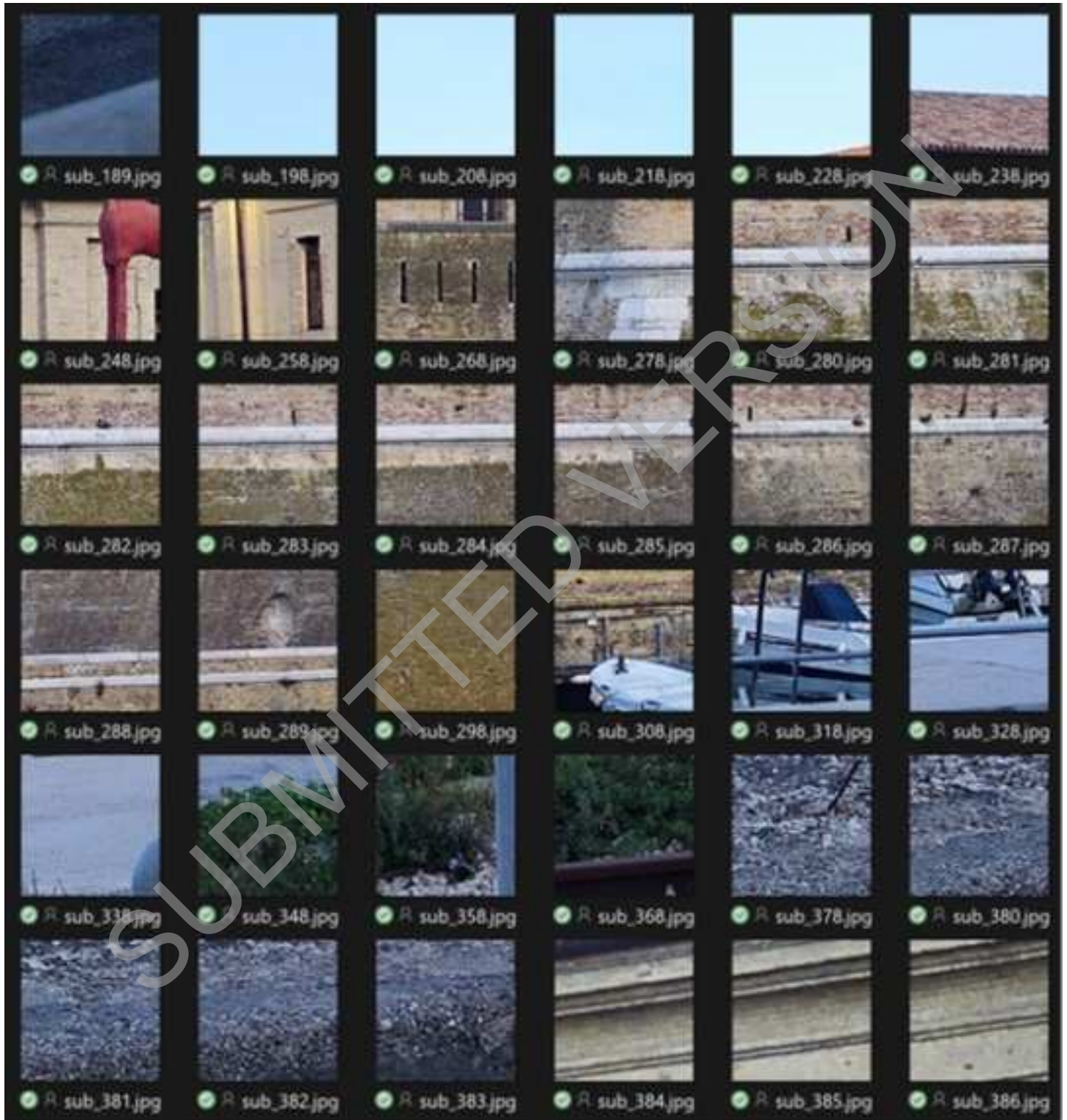


Figure 7







Brick Type	Colour
AR	light-red
AS	light red
B	dark red
CR	yellow
CS	yellow

SUBMITTED VERSION

Total porosity [%]	Roughness [μm]
19.24 ± 0.37	5.54 ± 0.42
19.24 ± 0.37	4.50 ± 0.27
24.62 ± 1.02	2.95 ± 0.63
44.09 ± 1.63	7.60 ± 0.57
44.09 ± 1.63	6.60 ± 0.49

SUBMITTED VERSION